JOURNAL OF MATERIALS SCIENCE 38 (2003) 4203–4210

# Photoanodic properties of ZnO thin films prepared from zinc acetate solutions containing cobalt acetate and polyvinylpyrrolidone

T. HIRANO, H. KOZUKA
*Department of Materials Science and Engineering, Kansai University, 3-3-35 Yamate-cho, Suita 564-8680, Japan*
*E-mail: kozuka@ipcku.kansai-u.ac.jp*

ZnO thin films were deposited on nesa silica glass substrates via sol-gel method using $Zn(CH_3COO)_2{\cdot}2H_2O$—$Co(CH_3COO)_2\cdot4H_2O$—polyvinylpyrrolidone (PVP)—diethanolamine—2-methoxyethanol solutions. The effects of the $Co^{2+}$ ions and PVP in coating solutions on the photoanodic properties of the resultant films were studied by measuring photocurrent—potential curves and action spectra in a three-electrode cell with a supporting electrolyte of pH = 9.18. The photoanodic current under xenon lamp light decreased with increasing amount of $Co^{2+}$ ions due to the decreased quantum efficiency in the UV regions. The photoresponse was extended to wavelengths of ca. 450 nm when the Co/Zn mole ratios were 0.05 and 0.15, while the response to the visible light diminished at Co/Zn > 0.3. The UV photoresponse of $Co^{2+}$-free ZnO films increased when PVP was added in the coating solutions, where the maximum quantum yield of 0.62 was obtained at a wavelength of 364 nm. On the other hand, the UV photoresponse rather decreased when PVP was added in $Co^{2+}$-containing solutions. © *2003 Kluwer Academic Publishers*

## 1. Introduction

Wet-type solar cells are regarded as ideal energy conversion system, which convert solar energy into electricity and chemical energy in the form of hydrogen gas without producing $CO_2$ gas. ZnO is one of the materials that have been extensively studied as photoanodes in wet-type solar cells [1]. ZnO has limited solar energy conversion efficiency, however, because of the large band gap (3.2 eV).

Jakani *et al*. prepared polycrystalline ZnO doped with 3d ions such as Cr, Mn, Fe, Co and Ni ions via conventional solid state reaction, measuring the action spectra in a three-electrode cell with aqueous solution of NaOH [2]. They found that the photoresponse extends to wavelengths of ca. 700 nm by doping ZnO with $Co^{2+}$ or $Ni^{2+}$. The doped samples had optical absorption peaks at 560, 620 and 650 nm, which were attributed to $^4A_2 \rightarrow {}^4T_1$ transitions. Bahadur and Rao prepared $Co^{2+}$-doped, polycrystalline ZnO films by spray pyrolysis, measuring the photoanodic properties in a three-electrode cell with acetonitrile solution of $NaClO_4$ [3]. They detected the photoresponse at 560, 620 and 650 nm as well as optical absorption, which they ascribed to $^4A_2 \rightarrow {}^4T_1$ transition. In both studies, Co/Zn mole ratios were limited under 0.05, and the quantum efficiency was not measured.

Keis *et al*. prepared ZnO layers with a variety of particle shape, porosity and thickness, examined the photoanodic properties in a three-electrode cell with aqueous solution of KI of pH 6.6 [4]. They found that the increase in porosity increases the quantum yield, obtaining the maximum yield of 0.9 in an 8 $\mu$m thick sample with specific surface area of 17.7 $m^2\ g^{-1}$, composed of particles 150 nm in size.

The literature shown above allow us to expect that larger amounts of $Co^{2+}$ ions could increase the photoresponse of ZnO in the visible region. It is also expected that porous, $Co^{2+}$-doped ZnO could have high quantum yield in the visible region. In the present study, preparation of $Co^{2+}$-doped ZnO films with larger Co/Zn ratios were attempted utilizing sol-gel method, and the photoanodic properties were studied. Second, the porosity was increased by adding an organic polymer, polyvinylpyrrolidone (PVP), in the coating solutions, expecting the increase in the photoresponse in the visible region.

## 2. Experimental

### 2.1. Sample preparation

$Zn(CH_3COO)_2{\cdot}2H_2O$ (Wako Pure Chemical Industries, Osaka, Japan), $Co(CH_3COO)_2{\cdot}4H_2O$ (Wako Pure Chemical Industries), $CH_3OC_2H_4OH$ (Wako Pure Chemical Industries), $NH(C_2H_4OH)_2$ (Wako Pure Chemical Industries), and PVP (Tokyo Kasei Kogyo, Tokyo, Japan, K-90) were used as the starting materials. Coating solutions were prepared at room temperature by adding and dissolving PVP, $NH(C_2H_4OH)_2$, $Zn(CH_3COO)_2{\cdot}2H_2O$ and $Co(CH_3COO)_2{\cdot}4H_2O$ in $CH_3OC_2H_4OH$ in this sequence. The molar compositions of the solutions are

TABLE I Compositions of the starting solutions

| Solution | Mole ratio | | | | |
|---|---|---|---|---|---|
| | $Zn(CH_3COO)_2{\cdot}2H_2O$ | $Co(CH_3COO)_2{\cdot}4H_2O$ | PVP | DEA | $CH_3OC_2H_4OH$ |
| Series 1 | | | | | |
| A | 1 | 0 | 0 | 1 | 17 |
| B | 1 | 0.05 | 0 | 1 | 17 |
| C | 1 | 0.15 | 0 | 1 | 17 |
| D | 1 | 0.3 | 0 | 1 | 17 |
| E | 1 | 0.5 | 0 | 1 | 17 |
| F | 1 | 1 | 0 | 1 | 17 |
| G | 1 | 2 | 0 | 4 | 68 |
| Series 2 | | | | | |
| A | 1 | 0 | 0 | 1 | 17 |
| H | 1 | 0 | 0.3 | 1 | 17 |
| I | 1 | 0 | 0.5 | 1 | 17 |
| Series 3 | | | | | |
| B | 1 | 0.05 | 0 | 1 | 17 |
| J | 1 | 0.05 | 0.3 | 1 | 17 |
| K | 1 | 0.05 | 0.5 | 1 | 17 |
| Series 4 | | | | | |
| C | 1 | 0.15 | 0 | 1 | 17 |
| L | 1 | 0.15 | 0.3 | 1 | 17 |
| M | 1 | 0.15 | 0.5 | 1 | 17 |

shown in Table I, where the mole ratio of PVP to $Zn(CH_3COO)_2{\cdot}2H_2O$ is defined for the monomer of PVP.

Dip-coating was conducted on a nesa silica glass substrate ($40 \times 20 \times 1.2$ mm$^3$) at a substrate withdrawal speed of 3 cm min$^{-1}$. The resultant gel films were placed immediately in an electric furnace of 600°C, kept there for 10 min, and then cooled down in the ambient atmosphere. When the solutions containing PVP were used, the gel films were heated at 300°C for 10 min, and then at 600°C for 10 min.

## 2.2. Characterization

The film thickness was measured by a contact probe surface profilometer (Model SE3400, Kosaka Laboratory, Tokyo, Japan). For this measurement a part of the gel film was scraped off with a surgical knife before heat-treatment, and the film thickness was determined from the level difference between the coated part and the scraped part after heat-treatment.

Crystalline phases of the films were identified by X-ray diffraction measurement with an X-ray diffratometer (Model RTP300, Rigaku, Tokyo, Japan) using Cu $K_\alpha$ radiation and operating at 50 kV and 150 mA. Optical absorption spectra of the films were measured using a spectrophotometer (Model UV-2400PC, Shimadzu, Kyoto, Japan), where a bare nesa silica glass substrate was used as the reference. Microstructure of the film samples was observed using an FE-SEM (Model JSM-6330 FII, JEOL, Tokyo, Japan).

## 2.3. Measurement of the photoanodic properties

Photoanodic properties of the films were evaluated using a potentiostat (Model HZ3000, Hokuto Denko, Osaka, Japan) in a three-electrode cell that consists of the electrode sample, a platinized Pt electrode and SCE as the working, counter and reference electrodes, respectively, and of an $Na_2B_4O_7$ (Wako Pure Chemical Industries) buffer solution of pH 9.18 A. 500 W xenon lamp (Model UXL-500D-0, XB-50101AA-A, UI-502Q, Ushio Denki, Tokyo, Japan) was used for illuminating the electrode sample from the front side, where the light intensity was reduced down to 20% using an ND filter. For measuring the current-potential curves, the potential was scanned from −0.4 to 1.0 V vs. SCE at a rate of 20 mV s$^{-1}$.

Action spectra of the films were measured at a potential of 0.5 V vs. SCE, where the xenon lamp light was monochromatized with a monochromator (Model SPG-100, Shimadzu, Kyoto, Japan). For this measurement, first the films were illuminated for 10 s, and then the light was put off. The difference in current before and after putting off the light was taken as the photocurrent. The intensity of the monochromatized light was measured with an optical power meter (Model TQ8210, TQ82107, Advantest, Tokyo, Japan), and the quantum yield (IPCE) was calculated from the photocurrent and the incident light intensity.

Space charge capacities were evaluated at 1 kHz using the potentiostat and a frequency response analyzer (Model FRA-5020, NF Electronic Instruments, Kanagawa, Japan).

# 3. Results

## 3.1. Film thickness

Fig. 1a shows the relationship between the Co/Zn ratio and the thickness of the films prepared from solutions without PVP (Series 1 solutions, Table I). The thickness ranged from ca. 0.03 to 0.15 $\mu$m, increasing with increasing Co/Zn ratio. The thickness of the film at Co/Zn = 2.0 was as small as 0.05 $\mu$m because of the larger amounts of the solvent in the solution (Solution G, Table I).

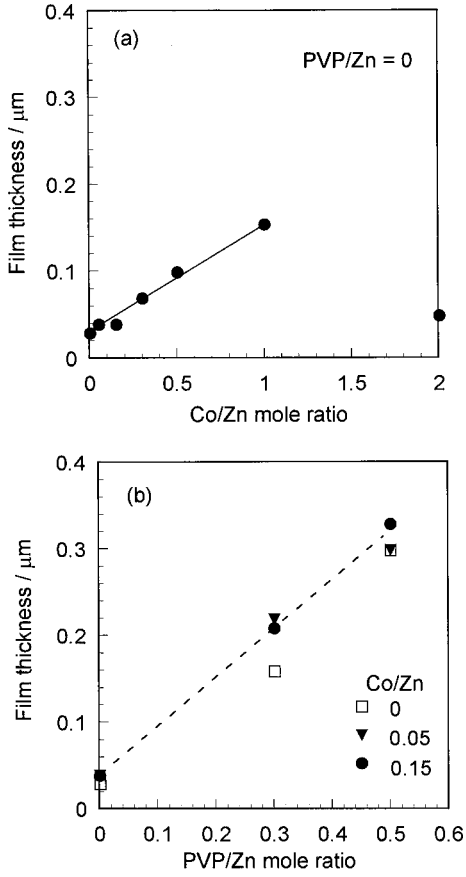


*Figure 1* Variation of the film thickness: (a) Co/Zn and (b) PVP/Zn ratios in the coating solutions. The films in (a) and (b) were prepared from Series 1 and Series 2–4 solutions, respectively.

Fig. 1b shows the relationship between the PVP/Zn ratio and the thickness of the films prepared from solutions of various PVP/Zn and Co/Zn ratios (Series 2–4 solutions). The thickness increased with increasing PVP/Zn ratio, achieving about 0.3 $\mu$m.

## 3.2. XRD patterns

Fig. 2a shows the XRD patterns of the films prepared from solutions of various Co/Zn ratios without PVP (Series 1 solutions). Only ZnO peaks were seen at Co/Zn = 0–0.15, and both ZnO and $ZnCo_2O_4$ peaks at Co/Zn = 0.3–1.0, where the intensity of the $ZnCo_2O_4$ peaks increased with increasing Co/Zn ratios. At Co/Zn = 2.0 only $ZnCo_2O_4$ peaks were detected.

Fig. 2b shows the XRD patterns of the films prepared from solutions of various PVP/Zn ratios at Co/Zn = 0.15 (Series 4 solutions). A trace amount of $ZnCo_2O_4$ was seen for PVP/Zn = 0.5.

## 3.3. SEM observations

Fig. 3 shows the SEM pictures of the films prepared from solutions of Co/Zn = 0 or 0.05 and PVP/Zn = 0 or 0.5. The samples prepared from solutions without PVP had relatively dense microstructure (Fig. 3a and b), which was not affected by the incorporation of cobalt. On the other hand, the incorporation of PVP in solutions increased the particle size and porosity as is seen in comparison between Fig. 3a and c and between Fig. 3b and d.

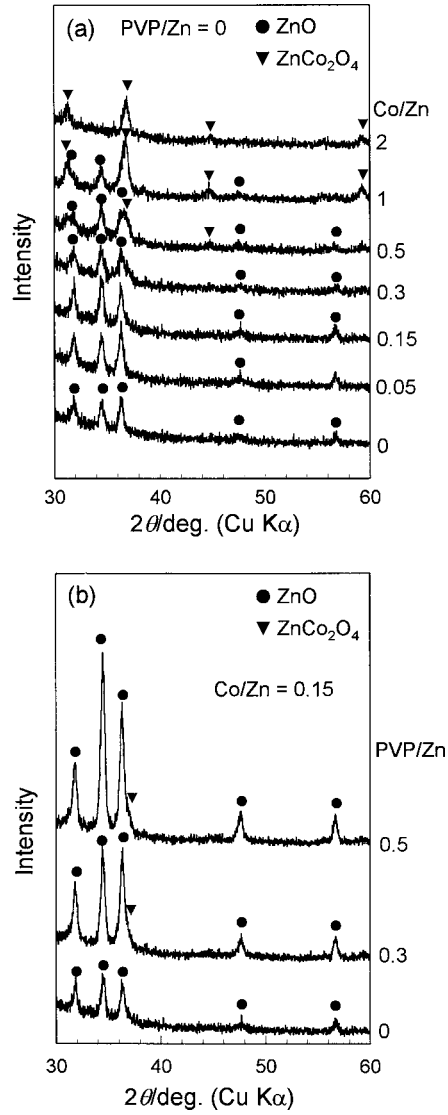


*Figure 2* XRD patterns of the films prepared from (a) solutions of various Co/Zn ratios without PVP (Series 1 solutions) and (b) solutions of various PVP/Zn ratios at Co/Zn = 0.15 (Series 4 solutions).

## 3.4. Optical absorption spectra

Fig. 4a shows the optical absorption spectra of the films prepared from solutions of various Co/Zn ratios without PVP (Series 1 solutions). The absorption coefficient, i.e., the absorbance divided by film thickness, is plotted on the vertical axis. It is seen that the absorption coefficient increased in the visible regions with increasing Co/Zn ratio. Particularly when Co/Zn $\geqq$ 0.3, the absorption coefficient at 400–500 nm predominantly increased with increasing Co/Zn ratio.

Fig. 4b shows the optical absorption spectra of the films prepared from solutions of various PVP/Zn ratios and of Co/Zn = 0.05 (Series 3 solutions). Significant variation in spectra was not observed in the visible region when the PVP/Zn ratio in solution was changed.

## 3.5. Current-potential curves

Fig. 5 shows the current-potential curves of the films prepared from solutions of various Co/Zn ratios without PVP (Series 1 solutions), measured under the xenon

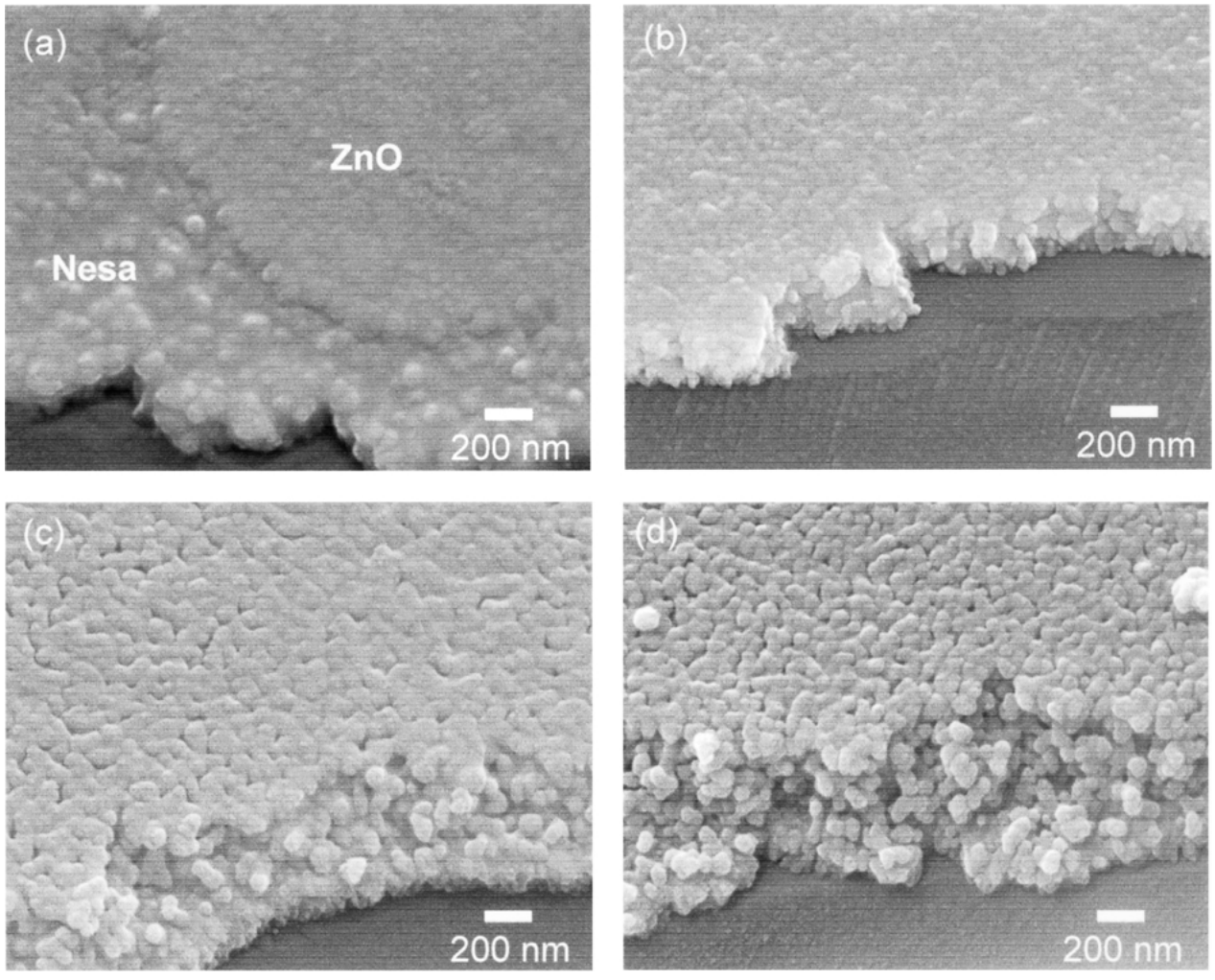


*Figure 3* SEM pictures of the films prepared from solutions of: (a) Co/Zn = 0 and PVP/Zn = 0 (Solution A), (b) Co/Zn = 0.05 and PVP/Zn = 0 (Solution B), (c) Co/Zn = 0 and PVP/Zn = 0.5 (Solution I) and (d) Co/Zn = 0.05 and PVP/Zn = 0.5 (Solution K).

lamp light illumination. The difference between the light current (solid lines) and dark current (broken lines) is regarded as the photocurrent. As seen in the figure the photocurrent decreased with increasing Co/Zn ratio, and diminished at Co/Zn = 2, namely, in the $ZnCo_2O_4$ sample. The photocurrent onset potential shifted positively when the Co/Zn ratio increases.

### 3.6. Action spectra

Fig. 6 shows the action spectra of the films prepared from solutions of various Co/Zn ratios without PVP (Series 1 solutions), measured at a bias potential of 0.5 V vs. SCE. The sample showed photoresponse mainly in the UV regions, which decreased with increasing Co/Zn ratio. However, the photoresponse extended to wavelengths around 450 nm when the Co/Zn mole ratio was 0.05 and 0.15. As the Co/Zn mole ratio increased over 0.15, the photoresponse at 400–450 nm decreased again, diminishing at Co/Zn = 1.

Fig. 7 shows the action spectra of the films prepared from solutions of various PVP/Zn ratios (Series 2 and 3 solutions). The spectra are shown for the samples of Co/Zn = 0 and 0.05 in Fig. 7a and b, respectively. When the samples contained no $Co^{2+}$ ions (Fig. 7a), the quantum efficiency increased in the UV regions (<400 nm) with increasing PVP/Zn ratio, while that remained negligible in the visible regions (>400 nm). On the other hand, when the samples contained $Co^{2+}$ ions at Co/Zn = 0.05 (Fig. 7b), the quantum efficiency decreased in the UV regions (<400 nm) with increasing PVP/Zn ratio, while that remained unchanged in the visible regions (>400 nm).

### 3.7. Mott-Schottky plot

Fig. 8 shows the Mott-Schottky plot of the films prepared from solutions of Co/Zn = 0 and 0.15 without PVP (Solutions A and C). The flat band potential was found to be −0.8 and −0.6 V vs. SCE at Co/Zn = 0 and 0.15, respectively, shifting positively by introducing $Co^{2+}$ ions. Assuming that the dielectric constant is unchanged at 10 [5] with incorporating $Co^{2+}$ ions, the donor density $N_D$ was calculated from the slope of the plot using Mott-Schottky equation [6];

$$\frac{1}{C_{SC}^2} = \frac{2}{e\varepsilon\varepsilon_o N_D}\left(|V - V_f| - \frac{kT}{e}\right) \qquad (2)$$

where $C_{SC}$ is the space charge capacitance, $\varepsilon$ the dielectric constant of the film, $\varepsilon_o$ the dielectric constant of vacuum, $V$ the applied potential, $V_f$ the flatband potential, $k$ Boltzmann's constant and $T$ the temperature. $N_D$ was

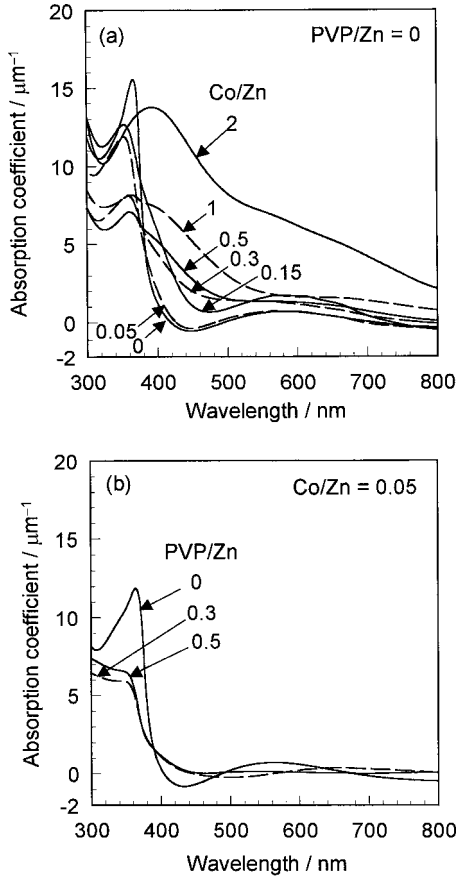


*Figure 4* Optical absorption spectra of the films prepared from: (a) solutions of various Co/Zn ratios without PVP (Series 1 solutions) and (b) solutions of various PVP/Zn ratios at Co/Zn = 0.05 (Series 3 solutions).

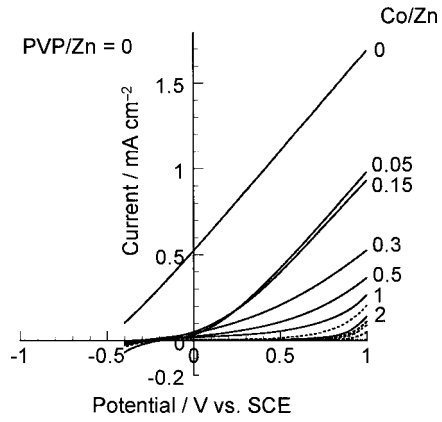


*Figure 5* Current-potential curves of the films prepared from solutions of various Co/Zn ratios without PVP (Series 1 solutions).

calculated to be $6.3 \times 10^{26}$ and $1.2 \times 10^{26}$ $m^{-3}$ at Co/Zn = 0 and 0.15, respectively, decreasing by introducing $Co^{2+}$ ions.

## 3.8. Photocurrent response curves

Fig. 9 shows the photoresponse curves of the films, obtained by plotting the current against time, where the monochromatic light of a wavelength of 364 nm was turned on, kept for 10 s, and then put off. The current was monitored at a bias potential of 0.5 V vs. SCE. For the undoped samples (Co/Zn = 0) the shape of the curve was not affected by introducing PVP in coating solutions.

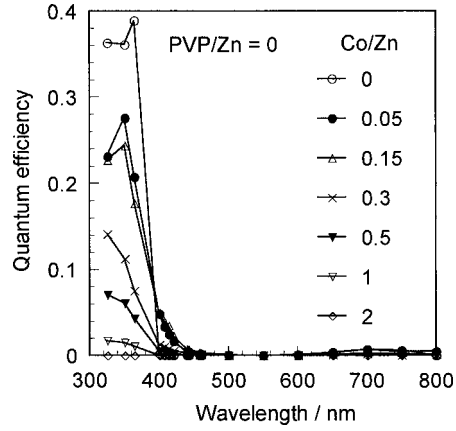


*Figure 6* Action spectra of the films prepared from solutions of various Co/Zn ratios without PVP (Series 1 solutions). The measurement was conducted at a bias potential of 0.5 V vs. SCE.

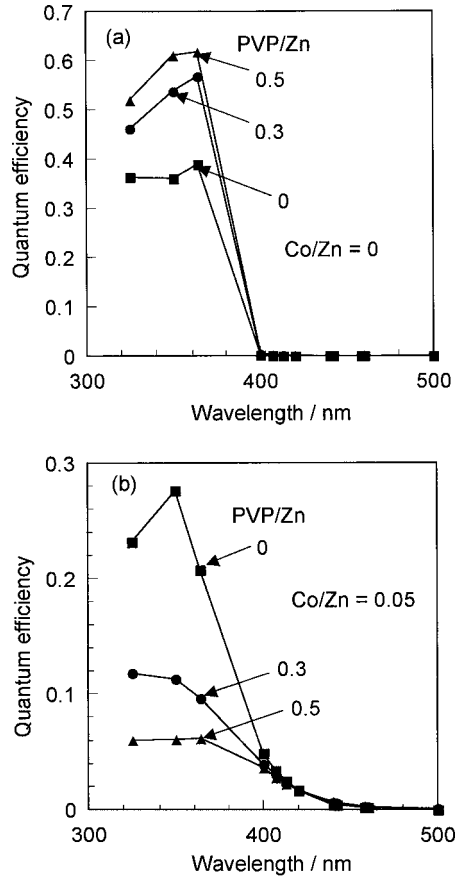


*Figure 7* Action spectra of the films prepared from solutions of various PVP/Zn ratios (Series 2 and 3 solutions). (a) Co/Zn = 0 and (b) Co/Zn = 0.05.

In contrast, for the $Co^{2+}$-doped samples (Co/Zn = 0.15) the shape of the curves changed by dissolving PVP in coating solutions. For the samples prepared from solutions containing no PVP, the photocurrent increased instantaneously on illumination, decreased exponentially. And on turning off the light, the current decreased instantaneously to negative values, and then decreased to zero exponentially. On the other hand, for the samples prepared from solutions containing PVP, the photocurrent increased rather gradually on illumination without showing exponential decay. And on turning off the light, the current gradually decreased to zero.

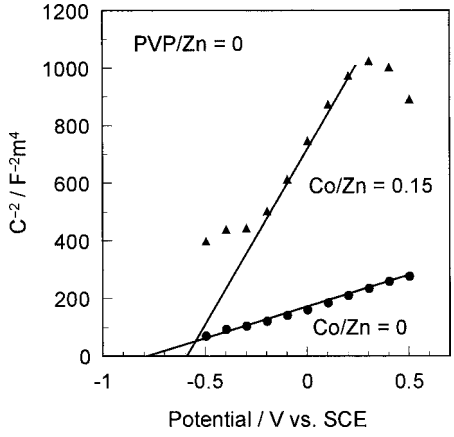


*Figure 8* Mott-Schottky plot of the films prepared from solutions of Co/Zn = 0 and 0.15 without PVP (Solutions A and C).

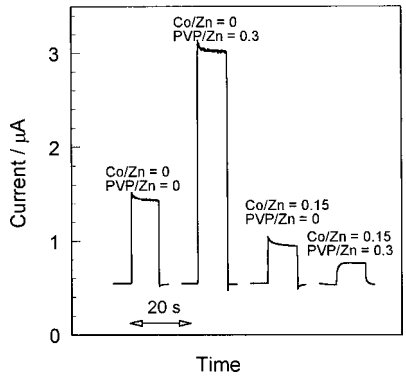


*Figure 9* Photoresponse curves of the films where the monochromatic light of λ = 364 nm was turned on, kept for 10 s, and then put off. The current was monitored at a bias potential of 0.5 V vs. SCE.

## 4. Discussion

### 4.1. Crystalline phases and optical absorption

The XRD patterns of the films prepared from solutions without PVP showed only ZnO peaks at Co/Zn = 0–0.15 (Fig. 2a), suggesting the formation of single-phase ZnO solid solutions. Because the ionic radii of tetrahedrally coordinated $Co^{2+}$ and $Zn^{2+}$ are quite similar at 0.072 and 0.074 nm [7], respectively, the absence of the XRD peak shift with Co/Zn ratio is reasonable. On the other hand, when PVP was added to the solution, the tendency of $ZnCo_2O_4$ phase segregation slightly increased as was seen for the samples prepared from solutions of Co/Zn = 0.15 (Fig. 2b).

The films prepared from solutions without PVP showed an increase in optical absorption at 500–700 nm with increasing Co/Zn up to 0.15 (Fig. 4a). When the Co/Zn ratio increased over 0.3, the absorption at shorter wavelengths also increased. Jakani *et al.* observed optical absorption bands at 520–700 nm for their $Co^{2+}$-doped ZnO, which was attributed to d-d transition of tetrahedrally coordinated $Co^{2+}$ ions [2]. The increase in absorption at 500–700 nm for the present films of Co/Zn = 0–0.15 is then attributed to the d-d transition of the $Co^{2+}$ ions substituted for $Zn^{2+}$ ions in ZnO lattice. $ZnCo_2O_4$ has normal spinel structure where $Co^{2+}$ ions are coctahedrally coordinated. This would be why the increase in absorption was observed also at shorter wavelengths for Co/Zn $\geqq$ 0.3.

### 4.2. Band models of the undoped ZnO and the $Co^{2+}$-doped ZnO thin films

ZnO is known as a direct gap semiconductor with a bandgap energy of 3.2 eV [8]. The flatband potentials of the undoped (Co/Zn = 0) and doped (Co/Zn = 0.15) films were found to be −0.8 and −0.6 V vs. SCE, respectively, as described in Section 3.7. On the basis of the bandgap energy and the flat band potentials, a band model was illustrated in Fig. 10 for the undoped ZnO and $Co^{2+}$-doped ZnO thin films at a bias potential of 0.5 V vs. SCE. The standard potentials of the redox couples $H_2/H_2O$ and $H_2O/O_2$ are 0 and 1.23 V vs. SHE, respectively, which decreases with pH by 0.059 V, and the potential of SCE is 0.241 V vs. SHE. Then the redox potential of $H_2/H_2O$ and $H_2O/O_2$ at pH = 9.18 are calculated to be −0.78 and 0.45 V vs. SCE, respectively, both of which are denoted in the band model. The energy level of the $Co^{2+}$ ions illustrated in the band model is that obtained through DV-X$\alpha$ cluster molecular orbital calculation by Ohashi *et al.* [9].

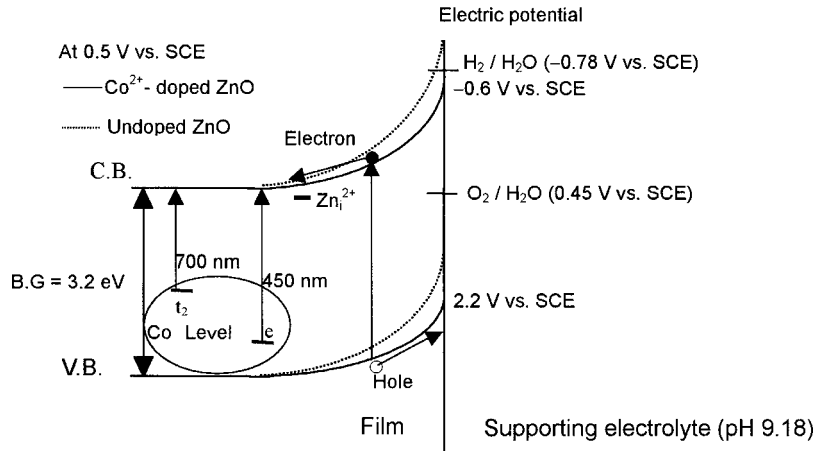


*Figure 10* Band model illustrated for undoped and $Co^{2+}$-doped ZnO thin films in a supporting electrolyte of pH = 9.18 at a bias potential of 0.5 V vs. SCE.

### 4.3. Effects of $Co^{2+}$ on the photoanodic properties of the films

The photocurrent under white light decreased with increasing Co/Zn ratio (Fig. 5), which is due to the decrease in quantum efficiency in the UV regions (Fig. 6). As described in Section 3.7, the Mott-Schottky plot (Fig. 8) indicated that the donor density decreases with increasing Co/Zn ratio, which would be the cause of the decreased quantum efficiency.

The current-potential curves (Fig. 5) and the Mott-Schottky plot (Fig. 8) also revealed that the flatband potential positively shifts with increasing Co/Zn ratio. The positive shift of the flatband potential decreases the slope of the band in the space charge layer as illustrated in the band model (Fig. 10). The decrease in the band slope can promote the electron-hole recombination, which can end up with reduction in quantum efficiency in the UV regions. Also $Co^{2+}$ ions on the surface of the electrodes can work as recombination centers as reported by Fichou [10]. They conducted time-resolved study of laser-induced open circuit photopotentials of $Co^{2+}$-doped sintered ZnO, finding that $Co^{2+}$ ions in tetrahedral sites act as recombination centers.

In summarizing, the introduction of $Co^{2+}$ ions decreases the donor density, decrease the slope of the band in the space charge region, and provide the recombination center, all of which are thought to reduce the quantum efficiency in the UV regions.

On the other hand, the quantum efficiency at 400–450 nm increased at Co/Zn = 0.05 and 0.15 (Fig. 6). Difference in energy between the conduction band and the $Co^{2+}$ ion e orbital is about 2.8 eV (Fig. 10) based on Ohashi *et al*.'s calculation [9]. This difference in energy corresponds to a wavelength of 450 nm, where an increase in quantum efficiency was observed (Fig. 6). Therefore, the photocurrent observed in the visible regions can be attributed to the excitation of electrons from the $Co^{2+}$ ion e orbital to the conduction band. In the samples of Co/Zn > 0.3 the quantum efficiency in the visible regions decreased again (Fig. 6). The XRD patterns (Fig. 2a) indicated that $ZnCo_2O_4$ are precipitated in these compositions, possibly providing the scattering sites for the electrons at $ZnO/ZnCo_2O_4$ interfaces.

### 4.4. Effects of PVP in coating solutions on the photoanodic properties of the films

#### *4.4.1. Undoped samples*

In the undoped samples (Co/Zn = 0), the quantum efficiency in the UV regions increased with increasing PVP/Zn ratios (Fig. 7a). The SEM pictures (Fig. 3a and c) indicated that that the films become porous by adding PVP in the coating solutions. An increase in porosity or specific surface area could provide larger reaction sites, leading to increased quantum efficiency. Similar observation was reported by Keis *et al*. [4], who prepared ZnO films by firing pastes of solution-derived ZnO powders and studied the photoelectrochemical properties, varying the morphology, porosity and film thickness. They found that the quantum efficiency increases with increasing specific surface area, and achieved the maximum quantum efficiency of 0.9 on a sample of specific surface area of 17.7 $m^2\ g^{-1}$.

An increase in the number of donors is also possible by addition of PVP. PVP in gel films is thermally decomposed and oxidized on firing. ZnO is known as a semiconductor having excessive cations, i.e., $Zn^{2+}$ in interstitial sites, which act as the donors. Oxidation of PVP would remove the $O^{2-}$ ions in the lattice, leading to increase in the number of $Zn^{2+}$ ions in the interstitial sites. The increase in interstitial $Zn^{2+}$ ions can increase the donor density, possibly leading to the increased quantum efficiency.

In summarizing, the increase in the specific area and donor density would be possible causes for the increased quantum efficiency provided by PVP.

#### *4.4.2. $Co^{2+}$-doped samples*

In contrast to the undoped samples, the $Co^{2+}$-doped samples showed decrease in the quantum efficiency in the UV regions (<400 nm) when the PVP/Zn ratio increased (Fig. 7b). As shown in Fig. 9, the samples prepared from PVP-containing solutions showed rather sluggish response when the light was turned on and off, in contrast to the samples from solutions without PVP. Maruska and Ghosh studied the shape of the photoresponse curves on $TiO_2$ doped with various transition metal ions [11]. They thought that the gradual increase in photocurrent on turning on the light is due to deep traps in the band structure. Namely, when the light is turned on, the excited electrons fill the traps, and then the full photocurrent is achieved. When the light is turned off, the traps are slowly thermally emptied, resulting in currents long after cessation of excitation. The gradual increase and decrease in photocurrent (Fig. 9) suggest that the samples from PVP-containing solutions have larger number of traps in the band structure.

Fichou reported that $Co^{2+}$ ions either on the surface or in the depletion region of ZnO can work as recombination centers [10]. Increase in specific surface area by PVP is also thought to provide larger numbers of these recombination centers, decreasing the quantum efficiency in the UV regions.

In contrast to the UV regions, the quantum efficiency did not decrease at 400–450 nm when PVP/Zn ratio increased for the $Co^{2+}$-doped samples (Fig. 7b). Södergen *et al*. [12] measured the photoanodic current of porous $TiO_2$ films by illuminating the films from the front or rear side, finding that the quantum efficiency is larger on illumination from the rear side. They thought that in porous electrodes the excited electrons and holes are conducted by diffusion rather than by the slope of the potential in the space charge layer. In the case of the present samples, the porosity increased with increasing PVP/Zn ratio, and electron conduction might change from band slope-aided conduction to diffusion. Since the visible light can penetrate the electrode more deeply than the UV light, the visible light-excited electrons near the nesa film can be diffused and contribute to the photocurrent. This may why the visible light photoresponse did not decrease on increasing PVP/Zn ratio.

## 5. Conclusions

$Co^{2+}$-doped ZnO thin films were prepared on nesa silica glass substrates by sol-gel method using $Zn(CH_3\ COO)_2{\cdot}2H_2O$—$Co(CH_3COO)_2{\cdot}4H_2O$—PVP—$NH(C_2H_4OH)_2$—$CH_3OC_2H_4OH$ solutions, and the effect of the $Co^{2+}$ dopants and the addition of PVP in solutions on the photoelectrochemical properties of thin films were studied in a three-electrode cell with supporting electrolyte of pH = 9.18.

(1) ZnO single-phase samples were obtained at mole ratios Co/Zn = 0–0.15, and $ZnCo_2O_4$ was precipitated at Co/Zn $\geqq$ 0.3 when PVP was not added in the solutions. When PVP was added in the solutions, a trace amount of $ZnCo_2O_4$ was precipitated at Co/Zn = 0.15.

(2) The addition of PVP in solutions gave rise to porous nature of the films.

(3) The UV photoanodic response decreased with increasing Co/Zn ratio, leading to a decrease in photoanodic current under xenon lamp light illumination. The photoanodic response was extended to wavelengths of ca. 450 nm at Co/Zn = 0.05 and 0.15, while the response to the visible light diminished when Co/Zn $\geqq$ 0.3.

(4) Undoped ZnO films showed an increase in UV photoanodic response when PVP was added in solutions. The maximum quantum yield of 0.62 was achieved at a wavelength of 364 nm at PVP/Zn = 0.5. The $Co^{2+}$-doped ZnO films, on the other hand, exhibited a decrease in the UV photoanodic response when PVP was added in solutions.


## Acknowledgments

This work is financially supported by the Institute of Industrial Technology, Kansai University, and by High Technology Research Center of Kansai University.


## References


1. W. HIRSCHWARD, *Curr. Top. Mater. Sci.* **7** (1981) 143.
2. M. JAKANI, G. CAMPET, J. CLAVERIE, D. FICHOU, J. POULIQUEN and J. KOSSANYI, *J. Solid State Chem.* **56** (1985) 269.
3. L. BAHADUR and T. N. RAO, *Solar Energy Mater. Solar Cells* **27** (1992) 347.
4. K. KEIS, L. VAYSSIERES, H. RENSMO, S.-E. LINDQUIST and A. HAGFELDT, *J. Electrochem. Soc.* **148** (2001) A149.
5. "CRC Handbook of Chemistry and Physics," 79 ed., edited by D. R. Lide (CRC Press, Boca Raton, 1998) p. 12.
6. H. O. FINKLEA, in "Semiconductor Electrodes," edited by H. O. Finklea (Elsevier, Absterdam, 1988) Chap. 1.
7. R. D. SHANNON, *Acta Crystallogr.* **A32** (1976) 751.
8. T. YAO, in "Optoelectronics Materials Manual," edited by Optoelectronic Industry and Technology Development Association (Optronics, Tokyo, 1986) p. 24 (in Japanese).
9. N. OHASHI, S. TANAKA, T. TSURUMI, J. TANAKA and O. FUKUNAGA, *J. Ceram. Soc. Jpn.* **106** (1998) 914.
10. D. FICHOU, *J. Electroanal. Chem.* **215** (1986) 161.
11. H. P. MARUSKA and A. K. GHOSH, *Solar Energy Mater.* **1** (1979) 237.
12. S. SÖDERGREN, A. HAGFELDT, J. OKSSON and S. E. LINDQUIST, *J. Phys. Chem.* **98** (1994) 5552.



*Received 5 November 2002*
*and accepted 23 July 2003*